Acta Neuropathol (2013) 125:289–302
DOI 10.1007/s00401-012-1048-7

ORIGINAL PAPER

Tau pathology in frontotemporal lobar degeneration with *C9ORF72* hexanucleotide repeat expansion

Kevin F. Bieniek · Melissa E. Murray · Nicola J. Rutherford · Monica Castanedes-Casey · Mariely DeJesus-Hernandez · Amanda M. Liesinger · Matthew C. Baker · Kevin B. Boylan · Rosa Rademakers · Dennis W. Dickson

Received: 16 August 2012 / Revised: 17 September 2012 / Accepted: 18 September 2012 / Published online: 28 September 2012

Abstract An expanded GGGGCC hexanucleotide repeat in *C9ORF72* is the most common genetic cause of amyotrophic lateral sclerosis and frontotemporal lobar degeneration associated with TDP-43 pathology (FTLD-TDP). In addition to TDP-43-positive neuronal and glial inclusions, *C9ORF72*-linked FTLD-TDP has characteristic TDP-43-negative neuronal cytoplasmic and intranuclear inclusions as well as dystrophic neurites in the hippocampus and cerebellum. These lesions are immunopositive for ubiquitin and ubiquitin-binding proteins, such as sequestosome-1/p62 and ubiquilin-2. Studies examining the frequency of the *C9ORF72* mutation in clinically probable Alzheimer's disease (AD) have found a small proportion of AD cases with the mutation. This prompted us to systematically explore the frequency of Alzheimer-type pathology in a series of 17 FTLD-TDP cases with mutations in *C9ORF72* (FTLD-*C9ORF72*). We identified four cases with sufficient Alzheimer-type pathology to meet criteria for intermediate-to-high-likelihood AD. We compared AD pathology in the 17 FTLD-*C9ORF72* to 13 cases of FTLD-TDP linked to mutations in the gene for progranulin (FTLD-*GRN*) and 36 cases of sporadic FTLD (sFTLD). FTLD-*C9ORF72* cases had higher Braak neurofibrillary tangle stage than FTLD-*GRN*. Increased tau pathology in FTLD-*C9ORF72* was assessed with thioflavin-S fluorescent microscopy-based neurofibrillary tangle counts and with image analysis of tau burden in temporal cortex and hippocampus. FTLD-*C9ORF72* had significantly more neurofibrillary tangles and higher tau burden compared with FTLD-*GRN*. The differences were most marked in limbic regions. On the other hand, sFTLD and FTLD-*C9ORF72* had a similar burden of tau pathology. These results suggest FTLD-*C9ORF72* has increased propensity for tau pathology compared to FTLD-*GRN*, but not sFTLD. The accumulation of tau as well as lesions immunoreactive for ubiquitin and ubiquitin-binding proteins (p62 and ubiquilin-2) suggests that mutations in *C9ORF72* may involve disrupted protein degradation that favors accumulation of multiple different proteins.

Keywords Frontotemporal lobar degeneration · C9ORF72 · Ubiquitin · P62 · Ubiquilin-2 · Tau

Electronic supplementary material The online version of this article (doi:10.1007/s00401-012-1048-7) contains supplementary material, which is available to authorized users.

K. F. Bieniek · M. E. Murray · N. J. Rutherford · M. Castanedes-Casey · M. DeJesus-Hernandez · A. M. Liesinger · M. C. Baker · R. Rademakers · D. W. Dickson (✉)
Department of Neuroscience, Mayo Clinic, 4500 San Pablo Road, Jacksonville, FL 32224, USA
e-mail: dickson.dennis@mayo.edu

K. B. Boylan
Department of Neurology, Mayo Clinic, 4500 San Pablo Road, Jacksonville, FL 32224, USA

Introduction

There is increasing clinical, pathologic, and genetic evidence that frontotemporal lobar degeneration with TDP-43 pathology (FTLD-TDP) and amyotrophic lateral sclerosis (ALS) are parts of a disease spectrum. The neuropathologic features of FTLD-TDP include focal cortical atrophy in frontal and temporal association cortices with variable involvement of parietal lobe and basal ganglia, as well as neuronal loss, gliosis, and inclusions within both neurons and glia that are immunoreactive for TDP-43 [9]. Clinically, FTLD-TDP manifests in changes in behavior, personality,

and language with relatively sparing of perception and memory [17]. ALS is the most common form of motor neuron disease, characterized by progressive degeneration of both upper and lower motor neurons, and leading to spasticity, muscle weakness, paralysis, and death within 3–5 years of onset. About half of the patients with ALS have features of frontal subcortical executive impairment, while some degree of motor neuron impairment is relatively common in FTLD-TDP [31, 32, 43]. The presence of TDP-43 in neuronal and glial inclusions in both disorders suggests that they have shared disease mechanisms.

Prior to the discovery of *C9ORF72* hexanucleotide repeat mutation on chromosome 9p21 [11, 42] in both FTLD-TDP and ALS, there were few genetic commonalties between these two disorders. Almost all patients with mutations in the gene encoding progranulin (*GRN*) had FTLD-TDP, while mutations in the gene encoding TDP-43 (*TARDBP*) had ALS [44]. In addition to FTLD-TDP and ALS, mutations in *C9ORF72* are found in patients with features of both (FTLD-MND). It has been proposed that this disease spectrum be referred to as c9FTD/ALS. Recently, distinctive pathology has been reported that may be pathognomonic of c9FTD/ALS, including cytoplasmic and intranuclear inclusions, as well as dystrophic neurites in cerebellum and hippocampus that are immunoreactive for ubiquitin and ubiquitin-binding proteins, sequestosome-1 (p62) and ubiquilin-2 (Ubqln2), but not for TDP-43 [1, 8, 11, 37]. The presence of Ubqln2 immunoreactive lesions in c9FTD/ALS is notable since similar pathology was originally described in patients with mutations in the *UBQLN2* gene, a mutation that results in X-linked ALS and ALS/FTD [12].

In a recent report of a series of cases of c9FTD/ALS from the Mayo Clinic Jacksonville brain bank, we demonstrated clinical and pathological heterogeneity in c9FTD/ALS [37]. Several elderly patients in our series had amnestic dementia rather than frontal behavioral syndromes or motor neuron disease and carried clinical diagnoses of Alzheimer's disease (AD). Moreover, Alzheimer-type pathology was prominent in some, including one case that had neurofibrillary tangles (NFT) consistent with Braak Stage V–VI compatible with high-likelihood AD. We subsequently screened AD cases in our brain bank that had concomitant TDP-43 pathology for ubiquitin-immunoreactive inclusions in cerebellar granular neurons, of which one case was positive; this patient was the only one of 320 pathologically confirmed AD cases with TDP-43 pathology that had a mutation in *C9ORF72*. This finding raised the possibility that Alzheimer-type pathology might be more frequent than expected in c9FTD/ALS. To address this question, we systematically evaluated the Alzheimer-type pathology in a series of 17 FTLD-TDP cases with mutations in *C9ORF72* (FTLD-*C9ORF72*) compared to 13 cases of FTLD-TDP linked to mutations in the gene for progranulin (FTLD-*GRN*) and 36 cases of sporadic FTLD (sFTLD).

Materials and methods

Case material

All of the cases were submitted to the brain bank for neurodegenerative disorders at Mayo Clinic in Jacksonville, Florida. Inclusion criteria were the presence of available frozen and formalin-fixed, paraffin-embedded tissue. Twenty cases with the hexanucleotide repeat expansion in *C9ORF72* and a neuropathologic diagnosis of FTLD–TDP or ALS had been previously reported [37]. Eight of the c9FTD/ALS cases with a clinical or neuropathologic diagnosis of ALS were excluded from this series since the focus was on FTLD-TDP. Four recent cases with FTLD-*C9ORF72* that were not reported in the original series are also included. In addition to the cases with a neuropathologic diagnosis of FTLD-TDP, 320 cases with TDP-43 pathology and a neuropathologic diagnosis of intermediate-to-high-likelihood AD [21] were screened for mutations in *C9ORF72* using the repeat-primed polymerase chain reaction method. Of the 320 genetically screened cases, a single case had the hexanucleotide repeat mutation. This case was also found to be the only case with ubiquitin immunopositive inclusions in cerebellar internal granular cell layer neurons in a series of 283 pathologically confirmed AD cases (283/320 cases with available formalin-fixed paraffin-embedded tissue) that were screened for inclusions blinded to mutation status.

The cases in this study were from several sources—the State of Florida Alzheimer's Disease Initiative ($n = 30$); neurology clinics at Mayo Clinic Florida ($n = 13$); CurePSP|Society of Progressive Supranuclear Palsy brain bank ($n = 11$); referral to the Parkinson disease brain bank ($n = 5$); Florida Alzheimer's Disease Research Center ($n = 1$); Einstein Aging Study ($n = 1$); and neuropathology consultations ($n = 5$). Clinical information (age at death, sex, clinical diagnosis, disease duration, and family history) was obtained from available medical records. The left (usually) hemibrain was fixed in 10 % formalin and the right hemibrain was frozen at −80°. Formalin-fixed tissue was sampled with standardized dissection methods and embedded in paraffin blocks. Sampled sections include frontal, temporal, parietal, visual, motor, and cingulate cortices, hippocampus, amygdala, basal ganglia, thalamus, midbrain, pons, medulla, and cerebellum.

Genetic analyses

All FTLD-*C9ORF72* cases had hexanucleotide repeat expansion in *C9ORF72* using a repeat-primed polymerase

chain reaction method to detect expansions of the GGGGCC hexanucleotide, and for most cases, the expansion was confirmed with Southern blotting [11]. Thirteen FTLD cases with a mutation in the gene for progranulin (*GRN*) were included for comparison. All FTLD-TDP cases enrolled in the Mayo Jacksonville brain bank are screened for *GRN* mutations by Sanger sequence analysis as previously described [16]. Thirty-six sFTLD cases, negative for mutations in both *GRN* and *C9ORF72*, were included as another comparison group. All cases had apolipoprotein E (*APOE*) genotype determined using Taqman SNP genotyping assay, read on the 7900HT Fast Real Time PCR system, and genotype calls were made using the SDS v2.2 software (Applied Biosystems).

Microscopic pathology

Thioflavin-S fluorescent microscopy was used to count senile plaques (SP) and neurofibrillary tangles (NFT), as well as score the severity of cerebral amyloid angiopathy (CAA) in cortical, limbic, and cerebellar regions. The density and distribution of NFT were used to assign a Braak NFT stage [7] as in previous publications [38]. In addition to Braak NFT stage, a Thal amyloid phase [47] was also assigned based upon counts of SP with thioflavin-S fluorescent microscopy in six cortical regions, four sectors of the hippocampus and two subregions of the amygdala, as well as semiquantitative SP scores (none, mild, moderate and severe) in the basal ganglia and cerebellum. Because we do not routinely characterize SP in the midbrain, we used counts in hippocampal CA4 subfield as a surrogate, since CA4 plaques are highly correlated with brainstem plaques [47]. Cases were also categorized according to the presence and severity of Alzheimer-type pathology that takes into account both the density of cortical SP and the distribution NFT as follows: 0, no SP and Braak stage <IV; 1, senile changes of Alzheimer type (sparse non-neuritic cortical SP and Braak stage <IV); 2, pathological aging [13] (numerous non-neuritic SP sufficient to diagnose AD with Khachaturian criteria [27] and Braak stage <IV); 3, Alzheimer's disease (numerous cortical SP with at least moderate neuritic type SP and Braak stage IV or greater) [27]. The Alzheimer-type pathologic subtype correlates highly with both Braak NFT stage (Spearman $r = 0.26$, $p = 0.03$) and Thal amyloid phase ($r = 0.72$, $p < 0.0001$). Cerebrovascular pathology was assessed with a reproducible scoring scheme proposed by Jellinger [22]. Lewy bodies were assessed with α-synuclein immunohistochemistry [50] and argyrophilic grains were assessed with tau immunohistochemistry [48].

The neuropathologic assessment of FTLD included TDP-43 immunohistochemistry on at least frontal cortex, hippocampus and medial temporal lobe, basal ganglia with amygdala and hypothalamus, midbrain, and medulla [23]. All cases had screening for cerebellar inclusions with immunohistochemistry for ubiquitin or p62, or both. A TDP-43 pathologic subtype was assigned to each case based on a Mackenzie TDP-43 subtyping [33] based upon morphology and distribution of lesions in cortical and subcortical regions as validated by our group [23]. The Mackenzie subtypes correspond to so-called "harmonization" types according to the following: Type 1 = Type A; Type 2 = Type C; Type 3 = Type B [34]. It should be noted that the harmonization report did not describe cortical and subcortical distribution of TDP-43 pathology or provide operational methods for assessing the subtypes; however, for the sake of clarity, we will refer to our cases by the harmonization type.

Immunohistochemistry and immunofluorescence

Immunohistochemistry for Ubqln2 (M03-5F5, 1:60,000, Abnova, Taipei City, Taiwan), p62 (p62 lck ligand, 1:1,000, BD Bioscience, Franklin Lakes, NJ, USA), ubiquitin (Ubi-1, 1:60,000; Millipore, Billerica, MA, USA), and phosphorylated TDP-43 (ps409/410, 1:5,000, Cosmobio Co., Tokyo, Japan) was performed on sections from the cerebellum and hippocampus. Immunohistochemistry for phosphorylated tau (PHF-1, 1:1,000, Peter Davies, Albert Einstein College of Medicine), and Aβ (33.1.1, 1:1,000, Mayo Clinic) was performed on sections from the hippocampus. Immunohistochemistry was done on 5-μm thick sections cut from formalin-fixed paraffin-embedded blocks, deparaffinized in three 5-min washes in xylene, rehydrated with three 2-min washes in a graded series of ethanol (100, 100, 95 %), and thoroughly washed in dH_2O. All stains were processed on a DAKO AutostainerPlus (DAKO, Carpinteria, CA, USA) with the DAKO EnVision™ + System-HRP (diaminobenzidine), with normal goat serum (1:20 in TBST; Sigma, St. Louis, MO, USA) used to block nonspecific antibody binding, added to slides prior to the primary antibody.

Double-labeled immunofluorescence (IF) was performed on select cases using antibodies to Ubqln2 (NBP1-85639, 1:500, Novus Biologicals, Littleton, CO, USA; and M03-5F5, 1:500, Abnova), phosphorylated tau (CP13; 1:500; Peter Davies, Albert Einstein College of Medicine), and Ubqln1 (AP2176c, 1:50, Abgent, San Diego, CA, USA). Slides were deparaffinized, rehydrated, washed, and blocked with DAKO serum-free protein block before incubation with the primary antibodies overnight at 4 °C. The following day, the slides were incubated with Alexa Fluor 488 and 568 conjugated secondary antibodies (1:500, Molecular Probes, Eugene, OR, USA) for 1.5 h at room temperature, washed, and treated with a solution of Sudan Black for 2 min to block autofluorescence. Slides were

coverslipped using Vectashield-DAPI mounting medium (Vector Laboratories, Burlingame, CA, USA) and visualized on a Zeiss Axio Imager Z1 microscope (Carl Zeiss Microscopy, Jena, Germany).

Tau image analysis

Sections immunostained with PHF-1 antibody were scanned on an Aperio ScanScope XT slide scanner (Aperio Technologies, Vista, CA, USA) producing a high-resolution digital image. The regions included for image analysis were hippocampus and temporal cortex. Digital image analysis was performed using Aperio ImageScope software. Two regions of interest were outlined from each image: the CA1 sector of the hippocampus and the sulcal side of the cortical ribbon of the occipitotemporal gyrus. A color deconvolution algorithm was used to count the number of pixels that were strongly immunostained by the DAB chromogen (Supplementary Fig. 1). The output variable was percentage of strong positive staining (based on region of interest area).

Statistical analyses

SigmaPlot (version 11) was used for statistical analyses. Due to the small sample sizes, non-parametric Kruskal–Wallis analysis of variance (ANOVA) on ranks was performed on quantitative measures to assess differences in the median values. Post hoc pairwise comparisons were performed between each of the groups using a Mann–Whitney rank sum test. For categorical data (e.g., sex and *APOE* genotype), a Chi-squared (χ^2) test was used to compare group differences. Fisher's exact test was used on pairwise categorical data with counts under 5. Correlative analysis was performed using Spearman rank order correlation. Significance for all measures was considered to be $p < 0.05$.

Results

Demographics and clinical features

FTLD-TDP cases were divided into three groups: FTLD-TDP with *C9ORF72* hexanucleotide repeat expansion (FTLD-*C9ORF72*; $N = 17$), FTLD-TDP with *GRN* mutation (FTLD-*GRN*; $N = 13$), and sporadic FTLD-TDP without a known mutation (sFTLD; $N = 36$). Of the 66 cases, 27 had a final clinical diagnosis of frontotemporal dementia (9 FTLD-*C9ORF72*, 5 FTLD-*GRN*, 13 sFTLD), 4 had progressive nonfluent aphasia (3 FTLD-*GRN*, 1 sFTLD), and 4 had frontotemporal dementia with motor neuron disease (1 FTLD-*C9ORF72*, 3 sFTLD). Twenty-three had a final diagnosis of clinically probable AD (7 FTLD-*C9ORF72*, 4 FTLD-*GRN*, 12 sFTLD). Other antemortem clinical diagnoses included progressive supranuclear palsy ($N = 4$; 2 FTLD-*GRN*, 2 sFTLD), corticobasal syndrome ($N = 4$; sFTLD), Pick's dementia ($N = 3$; 2 FTLD-*GRN*, 1 sFTLD), Parkinson's disease dementia ($N = 3$; sFTLD), dementia with Lewy bodies ($N = 2$; FTLD-*C9ORF72*), and normal pressure hydrocephalus ($N = 1$; sFTLD). Of the four FTLD-*C9ORF72* cases with intermediate-to-high-likelihood Alzheimer-type pathology, three had a final clinical diagnosis of frontotemporal dementia and one had a diagnosis of clinically probable AD. All FTLD-*C9ORF72* cases had widespread TDP-43 pathology, and six FTLD-*C9ORF72* cases had additional degeneration of upper or lower motor neurons, or both. None of the FTLD-*C9ORF72* cases had significant cerebrovascular disease, while three FTLD-*GRN* and six sFTLD cases had significant cerebrovascular vascular disease, defined as the presence of more than one microinfarct, lacunar infarcts or subcortical arteriosclerotic leukoencephalopathy. Summary of FTLD-*C9ORF72* patient demographics, pathologic features, and genetics can be found in Table 1.

The three groups did not significantly differ in age at death, disease duration, or male-to-female ratio. Median age was 72 for FTLD-*C9ORF72*, 67 for FTLD-*GRN*, and 76.5 for sFTLD. Median disease duration was 7 years for FTLD-*GRN*, 6 years for FTLD-*C9ORF72*, and 6 years for sFTLD. There were 41 men (11 FTLD-*C9ORF72*, 7 FTLD-*GRN*, and 23 sFTLD) and 25 women (6 FTLD-*C9ORF72*, 6 FTLD-*GRN*, and 13 sFTLD).

The groups differed significantly ($p < 0.001$) in the frequency of recorded family history of degenerative disease defined as dementia, parkinsonism, or motor neuron disease. Given the brain bank referral basis of this series, some cases did not have information about family history and in only a subset of cases was family history collected in a systematic fashion. All of the FTLD-*GRN* cases had a positive family history (13/13) of neurodegenerative disease, while 3/17 FTLD-*C9ORF72* cases, and 9/36 sFTLD cases had a positive family history. Accordingly, the pairwise comparisons were significant ($p < 0.001$) for FTLD-*C9ORF72* versus FTLD-*GRN*, and for sFTLD versus FTLD-*GRN*, but not ($p = 0.86$) for FTLD-*C9ORF72* versus sFTLD.

Macroscopic findings

The median calculated brain weight (determined by doubling the weight of the fixed hemibrain) was 1,000 g in FTLD-*C9ORF72*, 900 g in FTLD-*GRN*, and 1,055 g in sFTLD. The brain weight was significantly lower in FTLD-*GRN* cases compared with sFTLD ($p < 0.001$) and compared with FTLD-*C9ORF72* ($p = 0.018$), but no difference between FTLD-*C9ORF72* and sFTLD ($p = 0.44$).

Table 1 Demographic, pathologic, and genetic features of 17 FTLD-*C9ORF72* cases

Case no.	Age at death	Sex	TDP type	Path type	Brain weight	Cortical atrophy	Clinical Dx	Braak stage	Thal phase	ATP	ApoE
9	55	F	B	FTLD-MND	1,080	F	FTD	II	0	0	33
10	61	F	A	FTLD-MND	680	F, T, P	FTD vs. PiD	V–VI	5	3	33
11	62	M	B	FTLD-MND	1,280	F, T, P, O	FTDbv	II	0	0	34
12	62	F	B	FTLD-MND	960	F, T	AD	0	0	0	23
13	74	F	B	FTLD-MND	1,140	F, T	DLB	0–I	1	1	23
14	70	M	A	FTLD-TDP	1,140	F, T	FTD	IV	3	3	34
15	72	M	A	FTLD-TDP	1,280	F, T	AD	II	0	0	33
16	74	M	A	FTLD-TDP	780	F	FTD vs. DLB	II–III	0	0	34
17	74	M	C	FTLD-TDP	1,208	F, T	AD	II–III	3	2	34
18	81	M	A	FTLD-TDP	1,000	F, T, P, O	AD vs. FTD	II	3	1	33
19	83	F	A	FTLD-TDP	1,020	F, T, P, O	AD	III	0	0	34
20	86	M	A	FTLD-TDP	940	F	DLB	II–III	0	0	33
21	71	M	A	FTLD-TDP	720	F, T, P	VaD vs. FTD	II–III	3	2	33
22	76	M	B	FTLD-TDP	1,140	F, T, P, O	AD	IV	0	0	33
23	80	M	A	FTLD-TDP	980	F, T, P, O	AD	V	5	3	33
24	65	F	A	AD	840	F, T, P	FTD	V	5	3	33
25	70	M	A	FTLD-MND	1,000	F, T, P	FTD-MND	I–II	3	2	34

Case numbers correspond to *C9ORF72* cases previously published in Murray et al. (Cases 9–20) [37]. Cases 21–25 have not been previously published. TDP type is based on the harmonization classification scheme [34]. Brain weight is measured in grams and calculated by doubling the weight of the formalin-fixed hemibrain. Clinical diagnosis is the final diagnosis the patient received. *APOE* number refers to the ε2, ε3, and ε4 allelic combination

APOE apolipoprotein E, *AD* Alzheimer's disease, *ATP* Alzheimer's type pathology, *DLB* dementia with Lewy bodies, *F* female or frontal, *FTD* frontotemporal dementia, *FTDbv* behavioral variant frontotemporal dementia, *FTLD* frontotemporal lobar degeneration, *M* male, *MND* motor neuron disease, *O* occipital, *P* parietal, *PiD* Pick's disease, *T* temporal, *TDP* TAR DNA-binding protein 43 kDa, *VaD* vascular dementia, *vs.* versus (differential clinical diagnosis)

The four cases of FTLD-*C9ORF72* with pathologically confirmed intermediate-to-high-likelihood AD were heterogeneous. The calculated brain weight ranged from 680 to 1,140 g. All cases had moderate-to-severe cortical atrophy of the frontal lobe, with variable involvement of the temporal lobe (2 cases), parietal lobe (2 cases) or occipital lobe (1 case). Two cases had preservation of the medial temporal lobe; one case had moderate atrophy; and one case had severe atrophy. All four cases had enlargement of the lateral ventricles, with variable degrees of dilation of frontal and temporal horns. There were differences in subjective assessment of the thickness of cortical ribbon, with one case appearing normal and others having thinning (Fig. 1). All four cases also had some degree of atrophy of the hippocampus and amygdala. One case had mild atrophy of the basal ganglia; and two cases had mild atrophy of the thalamus. Pigmentation of the substantia nigra and locus ceruleus was variable, from none-to-moderate. All cases with pathologically confirmed AD had a normal appearing cerebellum.

Microscopic findings

All cases in this study had TDP-43 pathology, with 11 FTLD-*C9ORF72* classified as Type A, one case Type C, and five cases classified as Type B. All 13 FTLD-*GRN* cases were Type A. For the sFTLD, 24 were Type A, one was Type C, and 11 were Type B.

One FTLD-*C9ORF72* case (Case 24) had initially been classified clinically and pathologically as AD with concomitant TDP-43, a not uncommon finding in a subset of AD [2]. This case had abundant NFT and neuritic type SP in both limbic (including hippocampus, Fig. 2) and cortical regions consistent with high-likelihood AD. This case was the only one identified in a genetic screen of 320 pathologically confirmed AD cases with TDP-43 pathology to have a hexanucleotide repeat expansion in *C9ORF72*. This case was also the only one of 283 cases of AD detected in a screen of the cerebellum with ubiquitin immunohistochemistry blinded to genetic information that had neuronal cytoplasmic inclusions (NCI) in the internal granular cell layer (Fig. 3a).

Subsequent investigation of other brain regions revealed TDP-43-negative inclusions characteristic of c9FTD/ALS (Fig. 3). Specifically, ubiquitin and ubiquitin-binding proteins p62 and Ubqln2 labeled frequent NCI as well as neuronal intranuclear inclusions (NII) in the granule cell layer of the cerebellum (Fig. 3a, c, e). These inclusions were negative for TDP-43 (Fig. 3g). As with other cases of

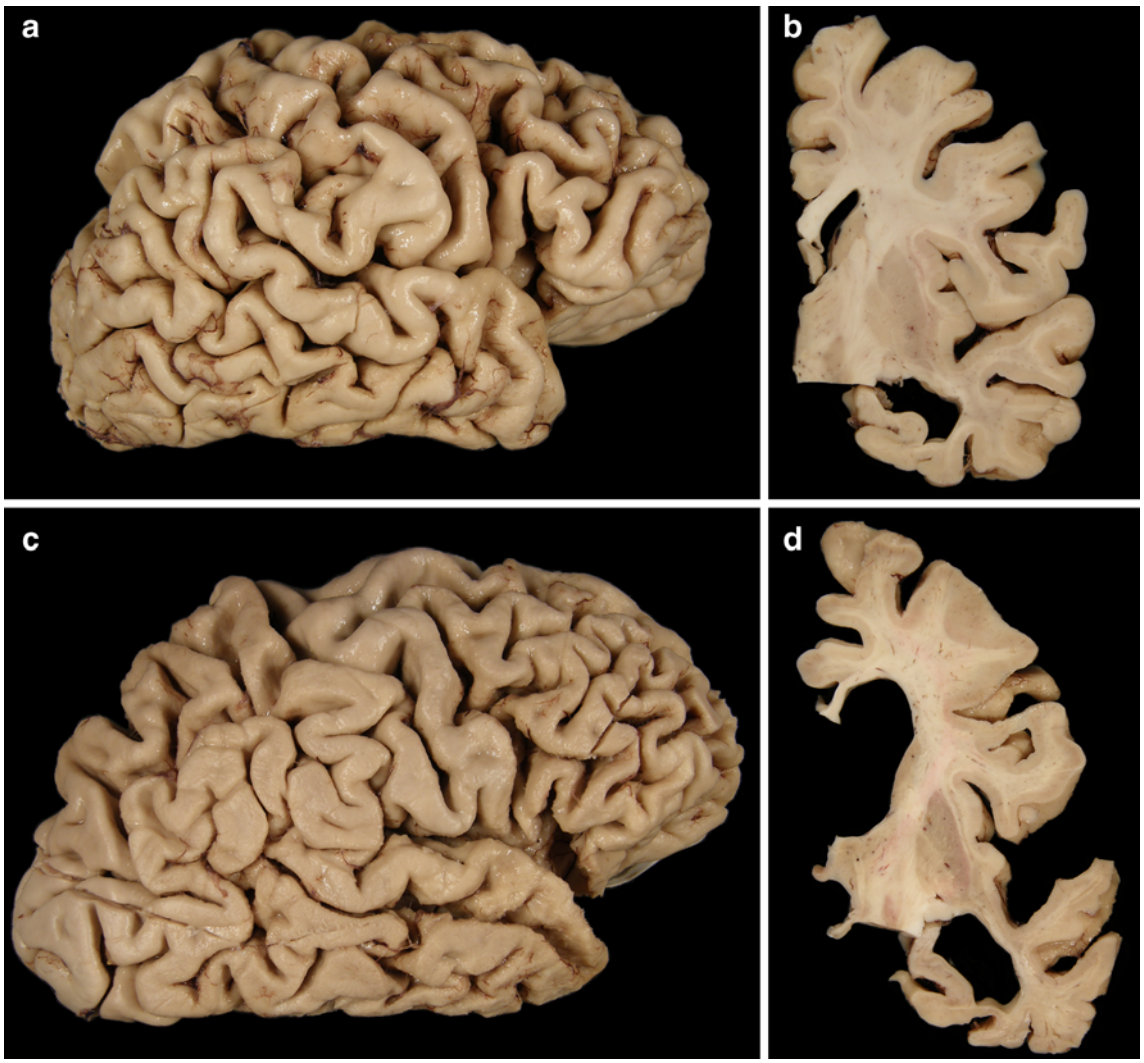

Fig. 1 Macroscopic comparison of two *C9ORF72* mutation carriers presenting with pathological AD (Case 24: **a**, **b**; Case 10: **c**, **d**). **a** Left hemisphere of AD/FTLD-U case with frontal, motor, and parietal cortical atrophy. **b** Coronal section at the level of the subthalamic nucleus shows widening of sulcal spaces, enlargement of the temporal horn of the lateral ventricle, and slight enlargement of the frontal horn of the lateral ventricle. **c** Right hemisphere of FTLD-TDP/AD case with frontal (predominantly frontal pole) "knife-edge" cortical atrophy as well as opercular and superior parietal atrophy. **d** Coronal section at the level of the subthalamic nucleus shows cortical atrophy and widening of sulcal space, thinning of the corpus callosum, and severe ventricular enlargement of the lateral ventricle

c9FTD/ALS, p62 labeled more inclusions than Ubqln2 or ubiquitin, and double labeling with Ubqln2 demonstrated that the inclusions were not always co-labeled (Supplementary Fig. 2). Ubiquitin and p62, but not Ubqln2, also labeled NCI in Purkinje cells (Fig. 3a, c, e), as well as glial cells in the molecular layer of the cerebellum (data not shown). In addition to specific c9FTD/ALS pathology, ubiquitin antibodies immunolabeled age-related granular degeneration of myelin in white matter [14], and both ubiquitin and p62 antibodies labeled NFT and dystrophic neurites in SP. In the hippocampus, ubiquitin, p62, and Ubqln2 antibodies labeled NCI in the dentate fascia (Fig. 3b, d, f). TDP-43-positive NCI were sparse compared to NCI labeled with ubiquitin and p62 (Fig. 3h). In the molecular layer and the endplate of the hippocampus, SP and NFT were labeled with ubiquitin and p62 antibodies, but not Ubqln2. Rather, Ubqln2 was a sensitive marker for FTLD-*C9ORF72*-related dystrophic neurites in the molecular layer of the dentate fascia, endplate and CA3, which could be traced to apical dendrites of these neurons.

Alzheimer-type pathology in FTLD-TDP

In FTLD-*C9ORF72*, eight cases had no Alzheimer-type pathology, two had mild senile changes, three had pathological aging, and four had neuropathology consistent with intermediate-to-high-likelihood AD. In FTLD-*GRN*, five had no Alzheimer-type pathology and eight had mild senile

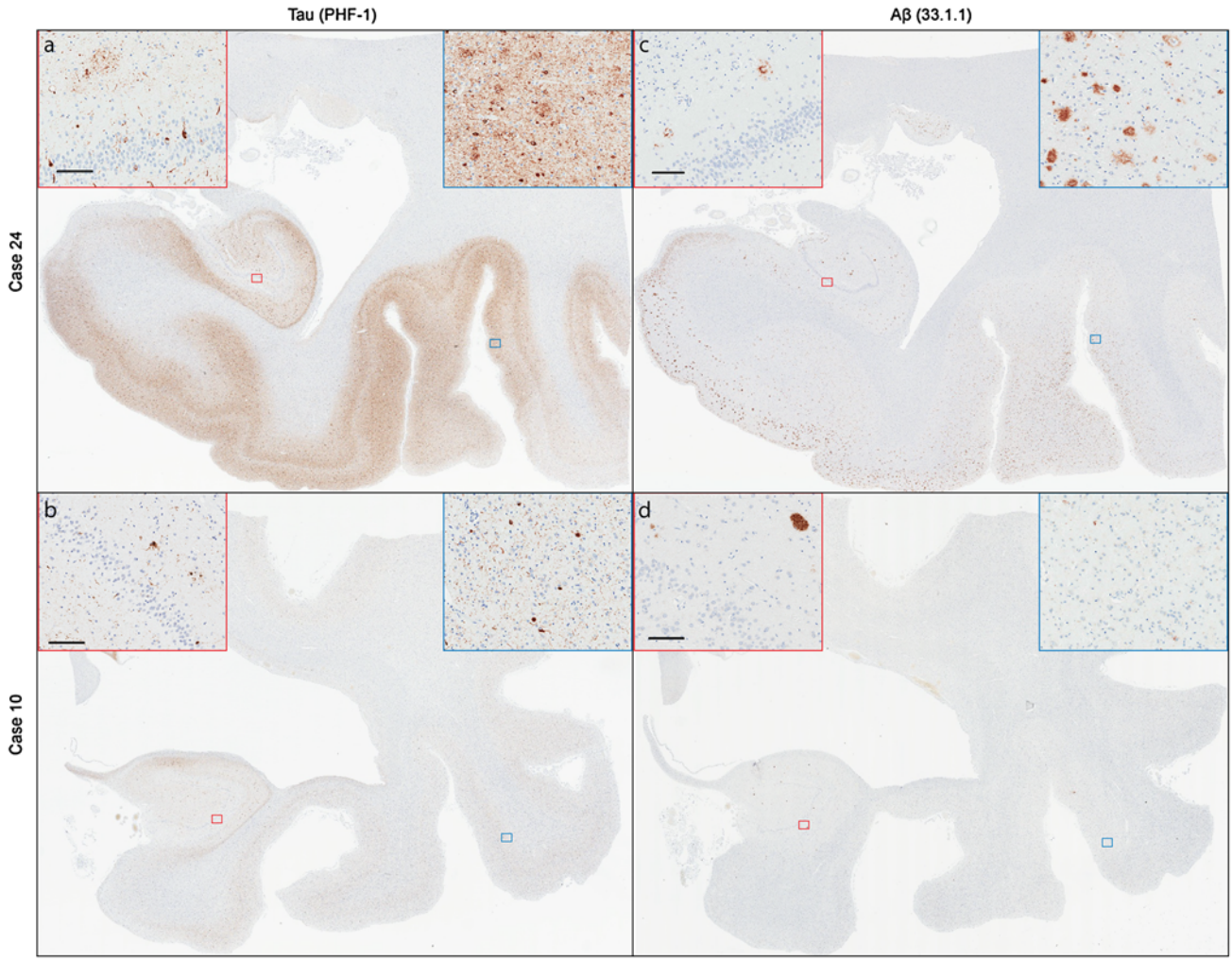

Fig. 2 Microscopic comparison of AD pathology in two *C9ORF72* mutation carriers presenting with pathological AD (Case 24: **a**, **c**; Case 10: **b**, **d**). Cases stained with a tau antibody (PHF-1; **a**, **b**) and an Aβ antibody (33.1.1; **c**, **d**). *Red inserts* show ×5 magnification of the hippocampus endplate, dentate fascia, and molecular layer. *Blue inserts* show ×5 magnification of the inferior temporal cortex. Case 24 has abundant tau and Aβ pathology in the hippocampus and temporal cortex consistent with Braak Stage V (**a**, **c**). While Case 10 has less overall tau and Aβ pathology in comparison to Case 24, the distribution of tangles is consistent with a similar Braak Stage V–VI (**b**, **d**). *Insert bar* 100 μm

changes. In sFTLD, 28 had no Alzheimer-type pathology and eight had pathological aging. Neither FTLD-*GRN* nor sFTLD had any individuals with intermediate-to-high-likelihood AD. Due to the low number of cases in some of the Alzheimer-type pathology classes, statistical comparison was only possible by combining cases with no Alzheimer-type pathology, mild senile changes, and pathological aging compared with cases with neuropathology of AD. Applying Fisher's Exact test in a pairwise manner revealed statistically significant difference between FTLD-*C9ORF72* and FTLD-*GRN* ($p = 0.008$), but not between FTLD-*C9ORF72* and sFTLD ($p = 0.113$). Other comparisons were not possible since no FTLD-*GRN* or sFTLD had neuropathology of AD. For Thal amyloid phase, there were no statistically significant differences amongst the FTLD-TDP groups or compared to age-matched cognitively normal controls (Table 2; Supplementary Tables 1 and 2). There were no differences in the frequency of *APOE* ε4 carrier state between the three groups (6/17 FTLD-*C9ORF72*, 3/13 FTLD-*GRN*, and 12/36 sFTLD).

On the other hand, statistically significant differences existed amongst the groups for Braak NFT stage (Table 2). FTLD-*GRN* had a median Braak NFT stage of 0, sFTLD had a median Braak NFT stage of II, and FTLD-*C9ORF72* had a median Braak NFT stage of II–III. Of the 17 FTLD-*C9ORF72* cases, five had Braak NFT stage IV or higher. Post hoc pairwise comparison between FTLD-*C9ORF72* and FTLD-*GRN*; FTLD-*C9ORF72* and sFTLD; and between FTLD-*GRN* and sFTLD, revealed p values of <0.001, 0.059, and <0.001, respectively. The results suggest that FTLD-*GRN* has lower

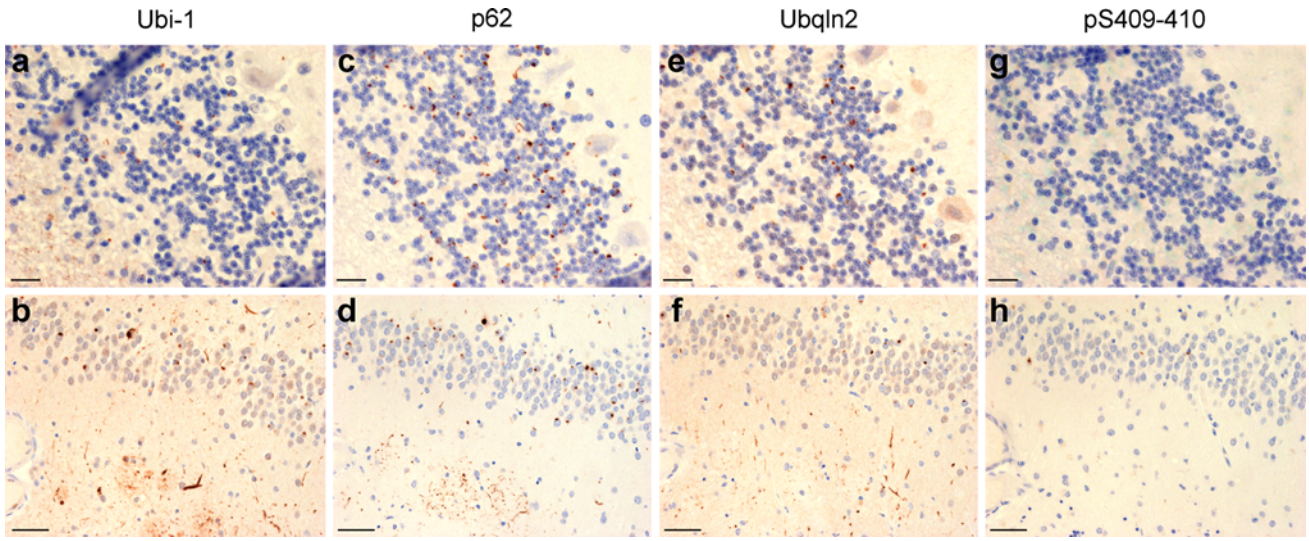

Fig. 3 Microscopic *C9ORF72* pathology in a pathological AD case. Ubiquitin (Ubi-1), sequestosome-1 (p62), ubiquilin-2 (Ubqln2), and phospho-TDP-43 (pS409/410) immunohistochemistry in the cerebellum (**a**, **c**, **e**, **g**) and hippocampus (**b**, **d**, **f**, **h**) of Case 24. Ubi-1 and p62 antibodies stain hallmark cerebellar NCIs in the Purkinje and granule cell layer, and hippocampal NCIs in the dentate fascia (**a**–**d**). Ubi-1 additionally labels normal aging pathology in the cerebellar white matter (unseen with p62), and senile plaques (SP) and neurofibrillary tangles (NFT) in the endplate and molecular layer of the hippocampus (**a**, **b**). p62 labels SP in the hippocampus (**d**). Ubqln2 marks cerebellar NCIs in the granule cell layer, but not in the Purkinje layer (**e**). In the hippocampus, the dentate contains Ubqln2-positive NCIs. The molecular layer has many immunopositive neurites and no Ubqln2-positive AD pathology (**f**; Fig. 4). There is no TDP-43 staining in the cerebellum and occasion TDP-43 stained NCIs in the dentate fascia (**g**, **h**). *Bar* = 20 μm for **a**, **c**, **e**, and **g**; 50 μm for **b**, **d**, **f**, and **h**

levels of tau pathology than both FTLD-*C9ORF72* and sFTLD, and that FTLD-*C9ORF72* tends to have increased tau pathology compared to sFTLD. A similar trend was seen when comparing these groups to age-matched cognitively normal controls (Supplementary Table 1).

To determine regional differences in SP and NFT pathology, we analyzed counts of SP and NFT from thioflavin-S fluorescent microscopy of various brain regions as described previously [38]. Between the three FTLD groups, there were no differences in the density of SP in the areas examined (Supplementary Table 2). For NFT, both the basolateral and corticomedial regions of the amygdala were different between FTLD-*C9ORF72* and FTLD-*GRN*, and between FTLD-*GRN* and sFTLD ($p = 0.050$ and $p = 0.009$, respectively). This finding was more marked when controlling for TDP-43 type (Table 2). In TDP-43 Type A cases (11/17 FTLD-*C9ORF72*, 13/13 FTLD-*GRN*, 24/36 sFTLD), only the CA2/3 of the hippocampus was different amongst the three groups for SP. In addition to the basolateral and corticomedial regions of the amygdala, the CA1, subiculum, nucleus basalis of Meynert, superior temporal cortex, and inferior parietal cortex were all statistically significant for NFT amongst the groups. Post hoc pairwise comparison revealed that all of the significant NFT regions had a difference between FTLD-*C9ORF72* and FTLD-*GRN*, none of these regions had a difference between FTLD-*C9ORF72* and sFTLD, and two regions (CA1 and amygdala) had a difference between FTLD-*GRN* and sFTLD. There were no differences amongst the FTLD-*C9ORF72* and sFTLD Type B cases (Supplementary Table 3), and there were too few Type C cases for statistical comparisons.

Phospho-tau image analysis in FTLD-TDP

Image analysis of phospho-tau in hippocampus and occipitotemporal gyrus was also used to assess quantitative differences in tau pathology between FTLD-*C9ORF72*, FTLD-*GRN* and sFTLD (Table 3). When cases were analyzed without reference to TDP-43 type, there were statistically significant differences between the groups in the occipitotemporal gyrus, but not the CA1 sector ($p = 0.034$ and 0.066, respectively). Post hoc pairwise comparison revealed significant differences between FTLD-*C9ORF72* and FTLD-*GRN* as well as sFTLD and FTLD-*GRN*, but not FTLD-*C9ORF72* and sFTLD ($p = 0.005$, 0.049, and 0.584, respectively). Limiting the analysis to only TDP-43 Type A cases showed a similar trend, with significant differences for occipitotemporal gyrus ($p = 0.026$) and for CA1 ($p = 0.020$), again between FTLD-GRN and the other two experimental groups. No significant differences were found between the FTLD-*C9ORF72* and sFTLD TDP-43 Type B cases.

Table 2 Comparison of senile plaques and neurofibrillary tangles in FTLD-*C9ORF72*, FTLD-*GRN*, and sFTLD

	FTLD			*p* value			
	C9ORF72 ($N = 11$)	GRN ($N = 13$)	Sporadic ($N = 24$)	All	C9 vs. GRN	C9 vs. sFTLD	GRN vs. sFTD
Age	72 (70, 81)	67 (64, 75)	81 (70, 84)	0.06			
Sex (M, F)	8, 3	7, 6	16, 8	0.60			
ApoE (ε4+, ε4−)	4, 6	3, 10	9, 15	0.61			
Braak NFT Stage	2.5 (2, 5)	0 (0, 0.6)	2 (1, 3)	<0.001*	<0.001*	0.06	<0.001*
Thal amyloid phase	3 (0, 4.5)	1 (0, 2.3)	1.5 (0, 3)	0.32			
Senile plaques							
CA1	0 (0, 2)	0 (0, 0)	0 (0, 0)	0.14			
CA2/3	0 (0, 0.8)	0 (0, 0)	0 (0, 0)	0.03*	0.06	0.05*	0.50
Subiculum	0 (0, 8)	0 (0, 0)	0 (0, 0)	0.10			
Amygdala BL	1 (0, 9)	0 (0, 1)	0 (0, 8)	0.41			
Amygdala CM	1 (0, 20)	0 (0, 3)	1 (0, 20)	0.17			
Average limbic SP	0.4 (0, 8)	0 (0, 2)	0.2 (0, 7)	0.36			
Midfrontal cortex	20 (0, 50)	0 (0, 3)	2 (0, 50)	0.07			
Superior temporal	2 (0, 44)	0 (0, 1)	0 (0, 30)	0.09			
Inferior parietal	3 (0, 50)	0 (0, 1.3)	12 (0, 43)	0.06			
Motor cortex	0 (0, 4)	0 (0, 0)	0 (0, 5)	0.20			
Visual cortex	3 (0, 26)	0 (0, 5)	3 (0, 14)	0.48			
Average cortical SP	9 (0, 33)	0.6 (0, 2)	5 (0, 30)	0.22			
Neurofibrillary tangles							
CA1	0 (0, 1)	0 (0, 0)	0 (0, 1.5)	0.04*	0.01*	0.74	0.02*
Subiculum	1 (0, 1)	0 (0, 0)	0 (0, 0.5)	0.02*	0.003*	0.18	0.06
Amygdala BL	1 (0, 2.5)	0 (0, 0)	0 (0, 2)	0.03*	0.01*	0.72	0.02*
Amygdala CM	1 (0.3, 2.8)	0 (0, 0)	0.5 (0, 2)	0.01*	0.001*	0.44	0.01*
Average limbic NFT	0.8 (0.3, 1.8)	0 (0, 0)	0.2 (0, 1)	0.001*	<0.001*	0.26	0.004*
Midfrontal	0 (0, 0.8)	0 (0, 0)	0 (0, 0)	0.14			
Superior temporal	0 (0, 1.8)	0 (0, 0)	0 (0, 0.8)	0.03*	0.01*	0.29	0.05
Inferior parietal	0 (0, 1.8)	0 (0, 0)	0 (0, 0)	0.05*	0.02*	0.15	0.13
Motor cortex	0 (0, 0)	0 (0, 0)	0 (0, 0)	0.28			
Visual cortex	0 (0, 0)	0 (0, 0)	0 (0, 0)	0.17			
Average cortical NFT	0 (0, 1.2)	0 (0, 0)	0 (0, 0.1)	0.03*	0.01*	0.21	0.06
Nucleus basalis of Meynert	3 (1, 8.5)	0 (0, 1)	1 (0, 3)	0.02*	0.01*	0.14	0.10
Cerebral amyloid angiopathy							
Midfrontal cortex	0 (0, 0.8)	0 (0, 0.3)	0 (0, 0)	0.89			
Motor cortex	0 (0, 0)	0 (0, 0)	0 (0, 0)	0.92			
Visual cortex	0 (0, 0.8)	0 (0, 0)	0 (0, 0)	0.80			
Average cortical CAA	0 (0, 0.3)	0 (0, 0.1)	0 (0, 0.3)	0.80			

The three groups in this table only include cases with Type A TDP-43 pathology. Sex and ApoE were analyzed with χ^2 analysis and are depicted with the number of cases in each category. All other variables analyzed with Kruskal–Wallis ANOVA on ranks and are depicted with the median, and lower and upper quartile values in parenthesis. Post hoc pairwise comparison analysis was performed with the Mann–Whitney rank sum test

BL basolateral, *C9* C9ORF72, *CAA* cerebral amyloid angiopathy, *CM* corticomedial, *ε4+* presence of at least one ε4 allele, *ε4−* absence of an ε4 allele, *F* female, *M* male, *NFT* neurofibrillary tangles, *SP* senile plaques

* Statistically significant *p* value ($p < 0.05$); All *p* value for ANOVA on ranks comparison of all three groups

Double-labeling immunofluorescence for phospho-tau

Evaluation of the spatial relationship between c9FTD/ALS-specific pathology, namely TDP-43-negative NCI and dystrophic neurites, and phospho-tau (PHF-1) pathology using immunofluorescence demonstrated minimal co-localization (Fig. 4a). Ubqln2-positive NCI in the dentate fascia and dendritic dystrophic neurites in the hippocampal

Table 3 Quantitative analysis of phospho-tau pathology in the CA1 and occipitotemporal gyrus in FTLD-*C9ORF72*, FTLD-*GRN*, and sFTLD

	CA1 median (Q1, Q3)	OCT median (Q1, Q3)
All TDP-43 types		
C9ORF72 ($N = 18$)	0.54 (0.23, 0.93)	0.47 (0.13, 2.0)
GRN ($N = 12$)	0.19 (0.11, 0.30)	0.10 (0.08, 0.20)
Sporadic ($N = 35$)	0.39 (0.21, 2.3)	0.43 (0.10, 1.6)
TDP-43 type A		
C9ORF72 ($N = 11$)	0.55 (0.27, 1.1)	0.50 (0.13, 3.0)
GRN ($N = 12$)	0.19 (0.11, 0.30)	0.10 (0.08, 0.20)
Sporadic ($N = 23$)	0.48 (0.22, 4.6)	0.65 (0.14, 3.0)
TDP-43 type B		
C9ORF72 ($N = 6$)	0.32 (0.08, 0.60)	0.43 (0.12, 0.81)
Sporadic ($N = 11$)	0.31 (0.15, 1.0)	0.19 (0.05, 0.68)
	p values	*p* values
All TDP-43 types		
All	0.06	0.03*
C9 vs. GRN	–	0.005*
GRN vs. sFTLD	–	0.05*
C9 vs. sFTLD	–	0.58
TDP-43 Type A		
All	0.02*	0.03*
C9 vs. GRN	0.01*	0.03*
GRN vs. sFTLD	0.02*	0.01*
C9 vs. sFTLD	0.91	0.98
TDP-43 Type B		
All	–	–
C9 vs. GRN	–	–
GRN vs. sFTLD	–	–
C9 vs. sFTLD	0.58	0.51

The three groups in this table are divided by cases with all TDP-43 pathology types (including 2 Type C cases), just Type A cases, and just Type B cases. The top panel contains the median value of the "percentage of strong positive staining" variable from the color deconvolution algorithm in both the CA1 and occipitotemporal cortex regions of interest as well as the lower and upper quartile values. The bottom panel contains the *p* values for the statistical analyses between all three groups ("All"; ANOVA on ranks), and the post hoc pairwise comparisons (rank sum test)

C9 C9ORF72, *OCT* occipitotemporal gyrus, *Q1* lower quartile (25 %), *Q3* upper quartile (75 %)

* Statistically significant *p* value ($p < 0.05$)

molecular layer had no phospho-tau, whereas phospho-tau-positive NFT in the dentate fascia and pyramidal layer, and the dystrophic neurites in SP in the molecular layer of the dentate fascia were not immunoreactive for Ubqln2. In contrast, Ubqln1, a closely-related protein to Ubqln2 and known ubiquitin-binding protein associated with NFT [35] showed little immunoreactivity with the *C9ORF72*-related pathology (Fig. 4b), but, there was a high degree of overlap between Ubqln1 and phospho-tau immunoreactive lesions.

Discussion

In the current study, we identified four patients with neuropathologic features of intermediate-to-high-likelihood AD who carried large *C9ORF72* hexanucleotide repeat expansions. Of these four cases, one was identified from a screen of 320 cases with a pathological diagnosis of intermediate-to-high-likelihood AD with concomitant TDP-43 pathology, and three were identified from 103 cases with a clinicopathologic diagnosis of FTLD. Twenty-five of the 103 FTLD cases had mutations in *C9ORF72* and three of these had concurrent Alzheimer-type pathology.

The nosologic significance of mixed Alzheimer and FTLD-TDP pathology is uncertain. TDP-43 pathology occurs in 25–50 % [2, 3, 20] of otherwise typical, albeit usually severe [25], AD. Conversely, Alzheimer-type pathologic features are found in FTLD-TDP in approximately 35 % of case [24]. Our four cases met pathologic criteria for both AD and FTLD-TDP. In the case identified from genetic and pathologic screening of AD cases with concomitant TDP-43 pathology (Case 24), we believe this case is primarily AD with secondary FTLD-TDP pathology, given multiple clinical and pathologic features that support this conclusion. First, a computerized tomography scan in 2003 and magnetic resonance imaging scans in 2003 and 2008 showed mild diffuse cerebral atrophy with no focal or lobar atrophy typical of FTLD. Second, on gross examination, in addition to diffuse cortical atrophy, there was also marked atrophy of the hippocampus as is common in AD. Third, there were numerous NFT and SP in the neocortex (frontal, temporal, parietal, and primary cortices), hippocampus, entorhinal cortex, basal nucleus of Meynert, hypothalamus, amygdala, and basal ganglia as well as mild amyloid angiopathy in the neocortex and cerebellum. Lastly, while there were TDP-43-immunopositive dystrophic neurites and NCIs, the extent of this pathology was modest compared with the degree of Alzheimer-type pathology and relatively limited in distribution. The three other cases with mixed Alzheimer and FTLD-TDP pathology (Cases 10, 14, and 23) had more clinical and pathological features suggestive of FTLD-TDP with concomitant Alzheimer-type pathology. These cases had more focal cortical atrophy and more widespread TDP-43 pathology. Additionally, the Alzheimer-type pathology was less pronounced compared with FTLD type pathology, which included not only widespread TDP-43-positive inclusions, but also p62- and Ubqln2-immunoreactive lesions.

To determine if Alzheimer pathology was specific to FTLD-*C9ORF72*, we examined FTLD-TDP cases due to

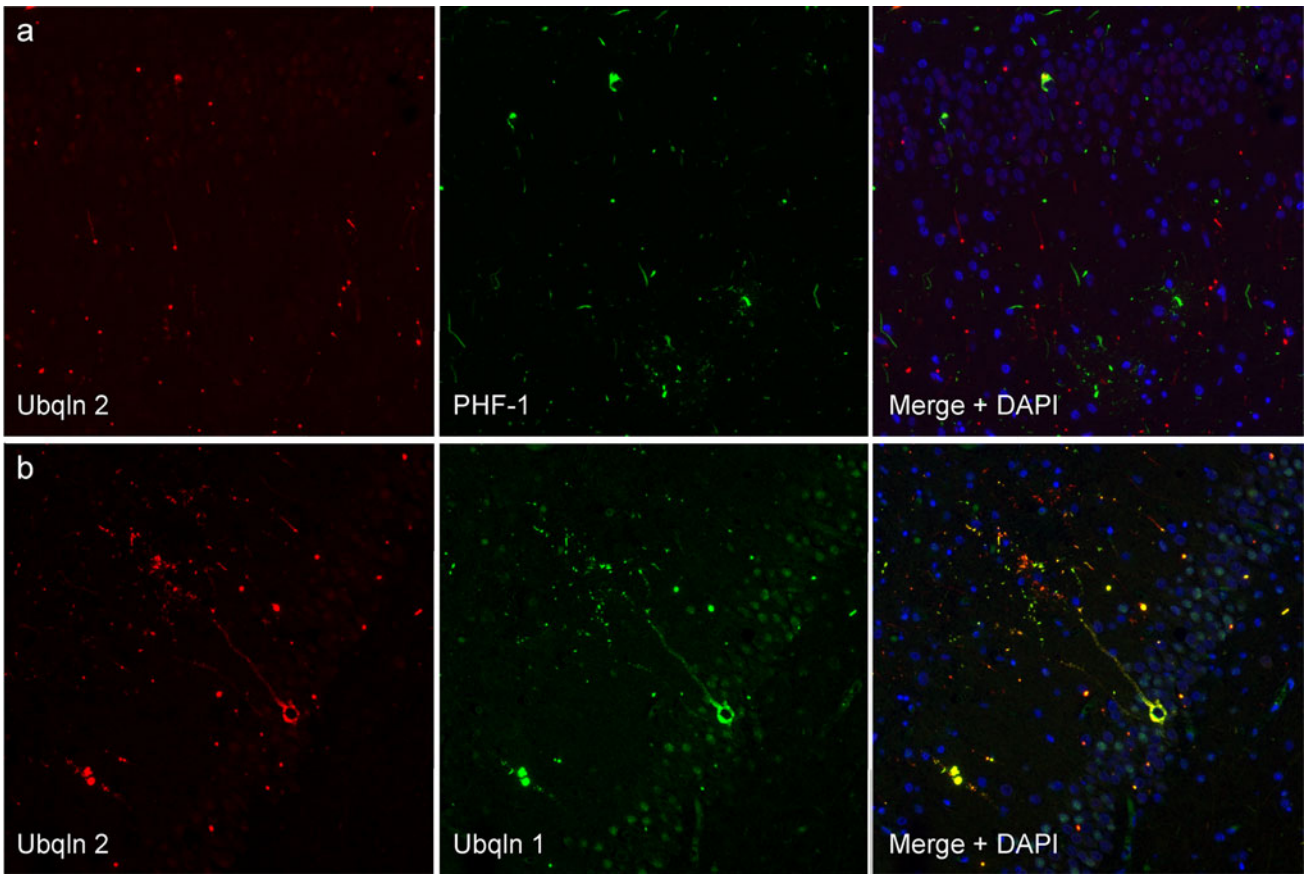

Fig. 4 Immunofluorescence in the hippocampus of a pathological AD case. **a** Double stain with Ubqln2 and phospho-tau (PHF-1) reveals comorbidity of *C9ORF72* pathology (neurites and NCIs) and AD pathology (plaques and tangles) with minimal colocalization. **b** Double stain with ubiquilin 1 (Ubqln1), a known marker of tangles, and Ubqln2 reveals co-labeled NCIs which could reflect sequence homology between the ubiquilins and poor antibody epitope specificity. While there are co-labeled puncta swellings in the molecular layer neurites, Ubqln1 does not label the entire process. Additionally, Ubqln1 labels a potential tangle in the dentate fascia; however, this neuron is also marked by Ubqln2 which is not known to stain tangles (Case 24, ×10 magnification)

another common genetic cause, mutations in the gene for progranulin (FTLD-*GRN*) as well as cases of FTLD-TDP that had no known disease-causing mutation (sFTLD). The three groups were similar with respect to age at death and male-to-female ratio, as well as *APOE* ε4 carrier state, indicating that any observed differences were unlikely to be related to these common risk factors for Alzheimer-type pathology [24]. The disease duration for the three groups was also similar (FTLD-*GRN*—7 years, FTLD-*C9ORF72*—6 years, sFTLD—6 years) and comparable to previously published reports [6, 19, 36, 45].

To assess Alzheimer-type pathology, we examined measures of tau pathology (Braak NFT stage, NFT counts) and amyloid pathology (Thal phase, SP counts). FTLD-*C9ORF72* cases had significantly higher Braak NFT stages compared to FTLD-*GRN* and a trend for higher NFT stage compared to sFTLD. There were no differences in distribution of amyloid plaques based upon thioflavin-S fluorescent microscopy as assessed by the Thal amyloid phase [47]. On the other hand, a summary measure for subtype of Alzheimer-type pathology (reflective of none, senile changes of AD type, pathological aging or intermediate-to-high likelihood of AD) was statistically different between FTLD-*C9ORF72* and sFTLD. In addition, comparison of regional counts of SP and NFT between the three groups showed higher median NFT counts in FTLD-*C9ORF72* in several brain regions, especially limbic lobe structures, but no differences in SP. Taken together, this data suggest that FTLD-*C9ORF72* may have a propensity for greater tau pathology than FTLD-*GRN*, and probably sFTLD, but not a similar propensity for Aβ pathology. These results fit with at least one other report that alluded to a greater tau than Aβ pathology in FTLD-*C9ORF72*. In particular, Hsiung and co-workers [19] found disproportionate degree of tau-immunopositive neurites in both cortical and limbic regions compared to Aβ pathology in three *C9ORF72*-linked FTLD cases. Another study by Mahoney and co-workers [36] found that cerebrospinal fluid Aβ in five cases of FTLD-*C9ORF72* had levels in the physiological range, but one of the cases had cerebrospinal

fluid tau levels outside of normal range. It should be noted, however, that cerebrospinal fluid tau levels are not specific and can be elevated in a range of neurologic disorders associated with neuronal damage [52].

Pathological heterogeneity of TDP-43 pathology is recognized in FTLD-TDP [23, 33], and we were concerned that TDP-43 subtype might play a role is susceptibility or resistance to Alzheimer-type pathology; therefore, we also analyzed group differences limited to cases with Type A pathology. With this analysis, differences in Alzheimer-type pathology were more marked. There were greater densities of NFT in the superior temporal and inferior parietal cortices, as well as all limbic regions studied in FTLD-*C9ORF72*. In an analysis limited to TDP–43 Type B, there were no differences between FTLD-*C9ORF72* and sFTLD cases (FTLD-*GRN* were all Type A), but the group sizes in this analysis were small and a false-negative result cannot be excluded.

Considering that many AD cases with TDP-43 pathology have Type A pathology [3, 51], it is perhaps not surprising that underlying tau pathology in FTLD-*C9ORF72* is more prevalent in Type A compared to other TDP-43 subtypes. It is interesting that quite similar to TDP-43 pathology in AD, tau pathology in FTLD-*C9ORF72* is more pronounced in the limbic regions (especially the amygdala) [3, 51]. In AD, TDP-43 pathology often co-localizes with tau pathology with respect to vulnerable brain regions, but also within individual neurons [2]. On the other hand, TDP-43-negative, ubiquitin/ubiquitin-binding protein pathology characteristic of FTLD-*C9ORF72* did not show significant co-localization with tau. In particular, there was clear separation of Ubqln2-positive NCI in the dentate fascia and elongated neuritic processes in the molecular layer compared with phospho-tau-positive NFT and dystrophic neurites of SP in the same sections.

To provide a more refined measure of tau pathology, high-resolution image analysis was used to assess phospho-tau burden in the CA1 sector of the hippocampus and in the occipitotemporal gyrus. The results confirmed those based on thioflavin-S fluorescent microscopy NFT counts. There was significantly greater tau burden in both FTLD-*C9ORF72* and sFTLD compared with FTLD-*GRN*, but no significant differences between FTLD-*C9ORF72* and sFTLD. Findings were similar, but more marked, when limited to TDP-43 Type A.

Ubiquitin-binding proteins bind to both ubiquitinated tau and other ubiquitinated proteins, like the ubiquitinated inclusions in FTLD. To determine if the ubiquilin family members differentially labeled tau and *C9ORF72*-linked inclusions, we used double-labeling fluorescence microscopy with antibodies to tau and to both Ubqln1 and Ubqln2. In a recent report by Brettschneider and co-workers [8], antibodies to Ubqln1 that did not recognize pan-ubiquilin epitopes did not strongly label NCI in dentate fascia, but did label neurites in the molecular layer of the dentate fascia. Our findings show a similar result. Overlap between the proteins was much greater between Ubqln1 and tau than between Ubqln2 and tau. Unlike the proprietary Ubqln1 antibody used by Brettschneider and co-workers, ours was a commercial antibody, and due to the high sequence similarity between the ubiquilin proteins, we believe the epitope specificity for the Ubqln1 antibody is not high. Ubqln1 was discovered as a protein that interacted with presenilin [35] and may be a chaperone for amyloid precursor protein that regulates Aβ secretion [18, 46], but is yet to be shown to have a direct role in tau pathophysiology, despite co-localization with tau immunoreactive neuronal lesions. Brettschneider and co-workers [8] reported that their Ubqln2 antibody, which is the same one we used, was cross-reactive with Ubqln1; however, we clearly showed differential labeling of Ubqln2 and Ubqln1 with respect to immunoreactivity of tau- and FTLD-*C9ORF72*-related lesions. Specifically, we detected sparse Ubqln1 immunoreactivity in NFT and dystrophic neurites of SP, but no such immunoreactivity for Ubqln2. Ultimately, antibodies with highly specific epitopes for each of the ubiquilin proteins expressed in the brain (Ubqln1, Ubqln2, and Ubqln4) need to be developed to further refine these distinctions.

Given greater tau pathology in both FTLD-*C9ORF72* and sFTLD compared with FTLD-*GRN*, it is reasonable to conclude that patients with FTLD-*GRN* are relatively resistant to Alzheimer-type tau pathology. On the other hand, reports of the hereditary dysphasic disinhibition dementia type 1 (HDDD1) with a c.5913 A>G mutation in *GRN* mutation have described Alzheimer pathology in four of five individuals that came to autopsy [5, 30]. These results contrast with experience with larger autopsy series containing a mixture of *GRN* mutations or series of cases with the same mutation. In one of the largest autopsy series, Rademakers and an international consortium reported mild Alzheimer-type pathology in only one of 13 subjects with the most common *GRN* mutation (R493X) [41] and in another autopsy series from the Mayo Clinic, Kelley and colleagues [26] reported moderate Alzheimer-type pathology in one of 13 subjects carrying a range (seven different mutations) of *GRN* mutations. Yet, in our autopsy series only FTLD-*C9ORF72* cases had severe Alzheimer-type pathology consistent with intermediate-to-high-likelihood AD. Until more is known about the function of c9orf72, it will be difficult to explain increase in tau pathology in FTLD-*C9ORF72*. Factors known to be associated with risk for Alzheimer-type pathology, including age, sex and APOE ε4 carrier state, did not account for this difference, since in FTLD-*C9ORF72* cases were similar to FTLD-*GRN* and sFTLD with respect for these parameters.

The underlying molecular mechanism accounting for the accumulation of ubiquitinated proteins in NCI and

dystrophic neurites in FTLD-*C9ORF72* remains unknown. The fact that these inclusions are immunoreactive for ubiquitin-binding proteins (p62 and Ubqln2) may suggest a mechanism linked to impairment in degradative processing of an unknown *C9ORF72*-related protein that accumulates in TDP-43-negative lesions [1, 8, 49]. Both p62 and another ubiquilin family member, Ubqln1, have also been shown to bind to ubiquitinated tau protein [28, 35]. Research by Babu and co-workers [4] has shown that p62 binds to K63-polyubiquitinated tau and is required for shuttling tau aggregates to the proteasome. Binding of p62 has also been shown to occur early in NFT formation and remains a consistent marker through NFT maturation [29]. Considering the ubiquitin-binding role of p62 with tau, it is conceivable that if p62 becomes sequestered by *C9ORF72*-related inclusions, and that insufficient p62 protein levels could lead to the secondary accumulation of hyperphosphorylated tau. On the other hand, this process does not account for amyloid deposition, the other major component of Alzheimer-type pathology.

Future research should compare Alzheimer-type pathology in FTLD-*C9ORF72* to other known genetic causes of FTLD, such as fused in sarcoma (*FUS*), valosin-containing protein (*VCP*), and charged multivesicular body protein 2B (*CHMP2B*). It is likely the FTLD-*FUS* and FTLD-*CHMP2B* will have a paucity of Alzheimer-type tau pathology similar to FTLD-*GRN* since initial descriptions of these disorders did not mention tau pathology [39, 40]. Conversely, pathologic descriptions of FTLD-*VCP* have mentioned AD and tau pathology, which is intriguing because VCP is also involved in the ubiquitin–proteasome system [10, 15, 53]. This would suggest that FTLD-*C9ORF72* may not be unique among genetically determined FTLD (aside from FTLD-*MAPT*) with respect to risk for tau pathology.

Acknowledgments We are grateful to all patients, family members, and caregivers who agreed to brain donation, without which these studies would have been impossible. We also acknowledge expert technical assistance of Linda Rousseau and Virginia Phillips for histology and John Gonzalez, Beth Marten, Pamela Desaro and Amelia Johnston for brain banking. This research was funded by Mayo Foundation (Jacoby Professorship of Alzheimer Research, Research Committee CR Program; ALS Center donor funds); National Institutes of Health (P50-AG16574, P50-NS72187, P01-AG03949, R01-AG37491, R01-NS65782 and R01-AG26251), CurePSP, The Society for Progressive Supranuclear Palsy; and the State of Florida Alzheimer Disease Initiative.

References

1. Al-Sarraj S, King A, Troakes C et al (2011) p62 positive, TDP-43 negative, neuronal cytoplasmic and intranuclear inclusions in the cerebellum and hippocampus define the pathology of C9orf72-linked FTLD and MND/ALS. Acta Neuropathol 122:691–702
2. Amador-Ortiz C, Lin WL, Ahmed Z et al (2007) TDP-43 immunoreactivity in hippocampal sclerosis and Alzheimer's disease. Ann Neurol 61:435–445
3. Arai T, Mackenzie IR, Hasegawa M et al (2009) Phosphorylated TDP-43 in Alzheimer's disease and dementia with Lewy bodies. Acta Neuropathol 117:125–136
4. Babu JR, Geetha T, Wooten MW (2005) Sequestosome 1/p62 shuttles polyubiquitinated tau for proteasomal degradation. J Neurochem 94:192–203
5. Behrens MI, Mukherjee O, Tu PH et al (2007) Neuropathologic heterogeneity in HDDD1: a familial frontotemporal lobar degeneration with ubiquitin-positive inclusions and progranulin mutation. Alzheimer Dis Assoc Disord 21:1–7
6. Boeve BF, Boylan KB, Graff-Radford NR et al (2012) Characterization of frontotemporal dementia and/or amyotrophic lateral sclerosis associated with the GGGGCC repeat expansion in C9ORF72. Brain 135:765–783
7. Braak H, Braak E (1991) Neuropathological staging of Alzheimer-related changes. Acta Neuropathol 82:239–259
8. Brettschneider J, Van Deerlin VM, Robinson JL et al (2012) Pattern of ubiquilin pathology in ALS and FTLD indicates presence of C9ORF72 hexanucleotide expansion. Acta Neuropathol 123:825–839
9. Cairns NJ, Bigio EH, Mackenzie IR et al (2007) Neuropathologic diagnostic and nosologic criteria for frontotemporal lobar degeneration: consensus of the Consortium for Frontotemporal Lobar Degeneration. Acta Neuropathol 114:5–22
10. Dai RM, Li CC (2001) Valosin-containing protein is a multi-ubiquitin chain-targeting factor required in ubiquitin-proteasome degradation. Nat Cell Biol 3:740–744
11. DeJesus-Hernandez M, Mackenzie IR, Boeve BF et al (2011) Expanded GGGGCC hexanucleotide repeat in noncoding region of C9ORF72 causes chromosome 9p-linked FTD and ALS. Neuron 72:245–256
12. Deng HX, Chen WJ, Hong ST et al (2011) Mutations in UBQLN2 cause dominant X-linked juvenile and adult-onset ALS and ALS/dementia. Nature 477:211–215
13. Dickson DW, Crystal HA, Mattiace LA et al (1992) Identification of normal and pathological aging in prospectively studied non-demented elderly humans. Neurobiol Aging 13:179–189
14. Dickson DW, Wertkin A, Kress Y, Ksiezak-Reding H, Yen SH (1990) Ubiquitin immunoreactive structures in normal human brains. Distribution and developmental aspects. Lab Invest 63:87–99
15. Forman MS, Mackenzie IR, Cairns NJ et al (2006) Novel ubiquitin neuropathology in frontotemporal dementia with valosin-containing protein gene mutations. J Neuropathol Exp Neurol 65:571–581
16. Gass J, Cannon A, Mackenzie IR et al (2006) Mutations in progranulin are a major cause of ubiquitin-positive frontotemporal lobar degeneration. Hum Mol Genet 15:2988–3001
17. Graff-Radford NR, Woodruff BK (2007) Frontotemporal dementia. Semin Neurol 27:48–57
18. Hiltunen M, Lu A, Thomas AV et al (2006) Ubiquilin 1 modulates amyloid precursor protein trafficking and Abeta secretion. J Biol Chem 281:32240–32253
19. Hsiung GYR, DeJesus-Hernandez M, Feldman HH et al (2012) Clinical and pathological features of familial frontotemporal dementia caused by C9ORF72 mutation on chromosome 9p. Brain 135:709–722
20. Hu WT, Josephs KA, Knopman DS et al (2008) Temporal lobar predominance of TDP-43 neuronal cytoplasmic inclusions in Alzheimer disease. Acta Neuropathol 116:215–220

21. Hyman BT, Trojanowski JQ (1997) Consensus recommendations for the postmortem diagnosis of Alzheimer disease from the National Institute on Aging and the Reagan Institute Working Group on diagnostic criteria for the neuropathological assessment of Alzheimer disease. J Neuropathol Exp Neurol 56:1095–1097
22. Jellinger KA, Attems J (2008) Prevalence and impact of vascular and Alzheimer pathologies in Lewy body disease. Acta Neuropathol 115:427–436
23. Josephs KA, Stroh A, Dugger B, Dickson DW (2009) Evaluation of subcortical pathology and clinical correlations in FTLD-U subtypes. Acta Neuropathol 118:349–358
24. Josephs KA, Tsuboi Y, Cookson N, Watt H, Dickson DW (2004) Apolipoprotein E epsilon 4 is a determinant for Alzheimer-type pathologic features in tauopathies, synucleinopathies, and frontotemporal degeneration. Arch Neurol 61:1579–1584
25. Josephs KA, Whitwell JL, Knopman DS et al (2008) Abnormal TDP-43 immunoreactivity in AD modifies clinicopathologic and radiologic phenotype. Neurology 70:1850–1857
26. Kelley BJ, Haidar W, Boeve BF et al (2009) Prominent phenotypic variability associated with mutations in Progranulin. Neurobiol Aging 30:739–751
27. Khachaturian ZS (1985) Diagnosis of Alzheimer's disease. Arch Neurol 42:1097–1105
28. Kuusisto E, Salminen A, Alafuzoff I (2001) Ubiquitin-binding protein p62 is present in neuronal and glial inclusions in human tauopathies and synucleinopathies. NeuroReport 12:2085–2090
29. Kuusisto E, Salminen A, Alafuzoff I (2002) Early accumulation of p62 in neurofibrillary tangles in Alzheimer's disease: possible role in tangle formation. Neuropathol Appl Neurobiol 28:228–237
30. Lendon CL, Lynch T, Norton J et al (1998) Hereditary dysphasic disinhibition dementia: a frontotemporal dementia linked to 17q21-22. Neurology 50:1546–1555
31. Lomen-Hoerth C, Anderson T, Miller B (2002) The overlap of amyotrophic lateral sclerosis and frontotemporal dementia. Neurology 59:1077–1079
32. Lomen-Hoerth C, Murphy J, Langmore S et al (2003) Are amyotrophic lateral sclerosis patients cognitively normal? Neurology 60:1094–1097
33. Mackenzie IRA, Baborie A, Pickering-Brown S et al (2006) Heterogeneity of ubiquitin pathology in frontotemporal lobar degeneration: classification and relation to clinical phenotype. Acta Neuropathol 112:539–549
34. Mackenzie IRA, Neumann M, Baborie A et al (2011) A harmonized classification system for FTLD-TDP pathology. Acta Neuropathol 122:111–113
35. Mah AL, Perry G, Smith MA, Monteiro MJ (2000) Identification of ubiquilin, a novel presenilin interactor that increases presenilin protein accumulation. J Cell Biol 151:847–862
36. Mahoney CJ, Beck J, Rohrer JD et al (2012) Frontotemporal dementia with the C9ORF72 hexanucleotide repeat expansion: clinical, neuroanatomical and neuropathological features. Brain 135:736–750
37. Murray ME, DeJesus-Hernandez M, Rutherford NJ et al (2011) Clinical and neuropathologic heterogeneity of c9FTD/ALS associated with hexanucleotide repeat expansion in C9ORF72. Acta Neuropathol 122:673–690
38. Murray ME, Graff-Radford NR, Ross OA et al (2011) Neuropathologically defined subtypes of Alzheimer's disease with distinct clinical characteristics: a retrospective study. Lancet Neurol 10:785–796
39. Neumann M, Rademakers R, Roeber S et al (2009) A new subtype of frontotemporal lobar degeneration with FUS pathology. Brain 132:2922–2931
40. Parkinson N, Ince PG, Smith MO et al (2006) ALS phenotypes with mutations in CHMP2B (charged multivesicular body protein 2B). Neurology 67:1074–1077
41. Rademakers R, Baker M, Gass J et al (2007) Phenotypic variability associated with progranulin haploinsufficiency in patients with the common 1477C → T (Arg493X) mutation: an international initiative. Lancet Neurol 6:857–868
42. Renton AE, Majounie E, Waite A et al (2011) A hexanucleotide repeat expansion in C9ORF72 is the cause of chromosome 9p21-linked ALS-FTD. Neuron 72:257–268
43. Ringholz GM, Appel SH, Bradshaw M et al (2005) Prevalence and patterns of cognitive impairment in sporadic ALS. Neurology 65:586–590
44. Rutherford NJ, Zhang YJ, Baker M et al (2008) Novel mutations in TARDBP (TDP-43) in patients with familial amyotrophic lateral sclerosis. PLoS Genet 4:e1000193
45. Simon-Sanchez J, Dopper EGP, Cohn-Hokke PE et al (2012) The clinical and pathological phenotype of C9ORF72 hexanucleotide repeat expansions. Brain 135:723–735
46. Stieren ES, El Ayadi A, Xiao Y et al (2011) Ubiquilin-1 is a molecular chaperone for the amyloid precursor protein. J Biol Chem 286:35689–35698
47. Thal DR, Rub U, Orantes M, Braak H (2002) Phases of A beta-deposition in the human brain and its relevance for the development of AD. Neurology 58:1791–1800
48. Togo T, Cookson N, Dickson DW (2002) Argyrophilic grain disease: neuropathology, frequency in a dementia brain bank and lack of relationship with apolipoprotein E. Brain Pathol 12:45–52
49. Troakes C, Maekawa S, Wijesekera L et al (2011) An MND/ALS phenotype associated with C9orf72 repeat expansion: Abundant p62-positive, TDP-43-negative inclusions in cerebral cortex, hippocampus and cerebellum but without associated cognitive decline. Neuropathology 32:505–514
50. Uchikado H, Lin WL, DeLucia MW, Dickson DW (2006) Alzheimer disease with amygdala Lewy bodies: a distinct form of alpha-synucleinopathy. J Neuropathol Exp Neurol 65:685–697
51. Uryu K, Nakashima-Yasuda H, Forman MS et al (2008) Concomitant TAR-DNA-binding protein 43 pathology is present in Alzheimer disease and corticobasal degeneration but not in other tauopathies. J Neuropathol Exp Neurol 67:555–564
52. van Harten AC, Kester MI, Visser PJ et al (2011) Tau and p-tau as CSF biomarkers in dementia: a meta-analysis. Clin Chem Lab Med 49:353–366
53. Watts GDJ, Wymer J, Kovach MJ et al (2004) Inclusion body myopathy associated with Paget disease of bone and frontotemporal dementia is caused by mutant valosin-containing protein. Nat Genet 36:377–381